Computational description of surface hydride phases on Pt(111) electrodes

Hanselman, S.R.; Calle Vallejo, F.; Koper, M.T.M.

Computational description of surface hydride phases on Pt(111) electrodes

Selwyn Hanselman, Federico Calle-Vallejo and Marc T. M. Koper

View Online   **Export Citation**   **CrossMark**

ARTICLES YOU MAY BE INTERESTED IN

AIP Publishing

Computational description of surface hydride phases on Pt(111) electrodes

Selwyn Hanselman,[1] (ID) Federico Calle-Vallejo,[2,3] (ID) and Marc T. M. Koper[1,a)] (ID)

AFFILIATIONS

[1] Leiden Institute of Chemistry, Leiden University, P.O. Box 9502, Leiden 2300 RA, The Netherlands

[2] Nano-Bio Spectroscopy Group and European Theoretical Spectroscopy Facility (ETSF), Department of Polymers and Advanced Materials: Physics, Chemistry and Technology, University of the Basque Country UPV/EHU, Av. Tolosa 72, 20018 San Sebastián, Spain

[3] IKERBASQUE, Basque Foundation for Science, Plaza de Euskadi 5, 48009 Bilbao, Spain

Note: This paper is part of the JCP Special Topic on Chemical Physics of Electrochemical Energy Materials.
[a)]Author to whom correspondence should be addressed: m.koper@chem.leidenuniv.nl

ABSTRACT

Surface platinum hydride structures may exist and play a potentially important role during electrocatalysis and cathodic corrosion of Pt(111). Earlier work on platinum hydrides suggests that Pt may form clusters with multiple equivalents of hydrogen. Here, using thermodynamic methods and density functional theory, we compared several surface hydride structures on Pt(111). The structures contain multiple monolayers of hydrogen in or near the surface Pt layer. The hydrogen in these structures may bind the subsurface or reconstruct the surface both in the set of initial configurations and in the resulting (meta)stable structures. Multilayer stable configurations share one monolayer of subsurface H stacking between the top two Pt layers. The structure containing two monolayers (MLs) of H is formed at −0.29 V vs normal hydrogen electrode, is locally stable with respect to configurations with similar H densities, and binds H neutrally. Structures with 3 and 4 ML H form at −0.36 and −0.44 V, respectively, which correspond reasonably well to the experimental onset potential of cathodic corrosion on Pt(111). For the 3 ML configuration, the top Pt layer is reconstructed by interstitial H atoms to form a well-ordered structure with Pt atoms surrounded by four, five, or six H atoms in roughly square-planar and octahedral coordination patterns. Our work provides insight into the *operando* surface state during low-potential reduction reactions on Pt(111) and shows a plausible precursor for cathodic corrosion.

Published under an exclusive license by AIP Publishing. https://doi.org/10.1063/5.0125436

I. INTRODUCTION

Cathodic corrosion is an intriguing process during which metals degrade under cathodic conditions and holds promise for the formation of catalytically active, low-dimensional materials from metal surfaces.[1–3] This process was accidently discovered by Haber in 1898 through aggregate formation from a Pt cathode during HCl electrolysis at strongly negative applied potentials.[1,4] However, the various uses of cathodic corrosion and its underlying mechanisms were not studied in detail until the last few decades when improved measuring methods and research toward novel catalysts sparked renewed interest,[1,5] including metals other than Pt or alloys.[2,6–9] During cathodic corrosion, part of the metal surface leaches into the medium, thereby forming nanoparticles and etching features on the surface. As the name implies, this occurs under highly negative

applied electrochemical potentials for Pt starting at ~−1.3 V vs the normal hydrogen electrode (NHE) (~−0.5 V vs reversible hydrogen electrode in alkaline media).[5,6]

The current hypothesis for the mechanism of this process is that the surface saturated with hydrogen atoms due to extreme reductive conditions forms platinum hydrides at the platinum–solvent interface that subsequently detach from the surface as $[PtH_n]^{m-}$, stabilized by electrolyte cations.[5,10,11] These strongly reducing complexes are subsequently oxidized by the aqueous medium to coalesce into suspended Pt clusters, nanoparticles, and aggregates. Since this process preferentially takes place on Pt(111),[5] a detachable platinum hydride can presumably be formed from an otherwise flat terrace.

Although in a recent computational paper, Evazzade *et al.* argued that cathodic corrosion of Pt(111) can occur through the presence of a single monolayer of adsorbed hydrogen (*H),[10]

cathodic corrosion occurs at potentials far beyond the onset of the hydrogen evolution reaction (HER). It is likely that cathodic corrosion is accompanied by more stable platinum hydride intermediates, forming subsurface multilayers rather than single surface adlayers. One allotrope of bulk platinum hydride, called PtH-II by Scheler et al., is known to be stable under partial pressures of $H_2(g)$ for bulk PtH of 27 GPa.[12,13] This pressure is equivalent to (only!) ~−0.16 V vs reversible hydrogen electrode (RHE) and hence may be formed under the electrochemical conditions observed for cathodic corrosion. However, free platinum hydride species are more readily formed from highly coordinated PtH_n moieties, i.e., with high n, exposed to the solvent medium. Forming platinum hydrides, which include such moieties, requires introducing high local densities of hydrogen into the surface, including beneath the first layer of platinum (subsurface), possibly exceeding 1 ML *H, or 1 H atom per Pt atom at the Pt(111)–liquid interface.

Subsurface hydrogen has been considered as a possible HER intermediate or side product.[14] Indeed, Stoerzinger et al. noted that irreversible or high-barrier adsorption of H—presumed to be a subsurface—takes place on Pt at ~−0.6 V vs RHE.[15] Such high-density Pt surface hydride structures are likely to be formed under the strongly reductive conditions necessary for cathodic corrosion. However, since the onset potential for cathodic corrosion is more negative than the onset for the hydrogen evolution reaction (HER), it is difficult to electrochemically discern between reduction processes and cathodic corrosion. Indeed, adsorption currents are obscured by HER currents, precluding the determination of both the degree of surface hydrogenation and any associated onset potentials. Moreover, the high HER activity on the surface impedes the structural analysis of the very structures necessary for cathodic corrosion,[10] and subsurface species likely present in the structure are less accessible to surface analysis methods.

Specific characterization of any surface hydride can be aided by using computational methods. Hong et al. and Légaré separately studied the vibrational and thermodynamic aspects, respectively, of both on-surface and subsurface H on Pt(111) using density functional theory (DFT).[16,17] Both studies concluded that *H may bind in subsurface sites up to 2 ML, corresponding to subsurface hydrogen at positive potentials with respect to the reversible hydrogen electrode (RHE).[16,17] However, this observation contradicts the experimental observation by Stoerzinger et al. of the subsurface hydrogenation process at significantly more negative potentials.[15] Moreover, both studies limited subsurface H adsorption to existing tetrahedral and octahedral sites in the fcc structure, while Scheler et al. suggested fcc-to-hcp reconstruction when reducing bulk Pt to PtH.[12] In addition, hydrogen coverages greater than 2 ML were not considered.[16,17] A more recent study by Mager-Maury et al. found stable $Pt_{13}H_n$ clusters to exist on γ-alumina for $n > 13$, up to Pt:H ratios of 1:3, accompanied by a significant reconstruction of the Pt cluster geometry and coincidence with modified binding to the surface.[18] If similar H coverages—3 ML H or greater—can be obtained through the modification of the surface layer of Pt(111) and the corresponding onset potentials are realistically negative yet sufficiently close to the potentials needed for HER, high-density H configurations may be a good description of the true structure (or even its precursor) of the surface on which cathodic corrosion of Pt takes place. Additionally, the HER behavior depends on the structure of

the surface, which is likely different when it is heavily hydrogenated at large overpotentials compared to the low-overpotential, more pristine metal surface.

Hence, in this study, we used computational methods—more specifically, DFT—to first obtain stable structures of high-H-density surface hydrides on Pt(111). Subsequently, we determined whether the formation of these platinum hydrides is thermodynamically favored at electrochemical potentials associated with cathodic corrosion and whether any thermodynamic barriers are involved in achieving such high coverages.

II. COMPUTATIONAL METHODS

A. General parameters and thermodynamic methods

Formation energies of various platinum hydrides were calculated using Vienna Ab initio Simulation Package (VASP) 5.4.4 and the DFT methods implemented therein.[19–22] The methods are generally in line with the methods described by Arulmozhi et al. to enable a comparison between <1 and >1 ML H surface hydrides.[23] All calculations were performed using the Perdew–Burke–Ernzerhof (PBE) exchange–correlation functional,[24] while the corresponding projector augmented-wave pseudopotentials were obtained from the VASP 5.4.4 distribution.[25,26] The wavefunction cutoff used in all calculations was 450 eV. Two types of simulation cells were used: cells that contain only H_2 used as a reference and slab cells that contain the Pt(111) surface and various hydrides derived from it. The simulation cell properties, global construction of the systems simulated within, and cell-specific computational parameters are described in Sec. II B.

DFT electronic energies E_{DFT} and local optima of atomic positions were obtained for each individual system by relaxing free atoms up to maximum atomic forces of 0.05 eV Å^{-1}. Depending on the system, this relaxation process may consist of multiple phases with different optimization algorithms, parameters, or mobile atoms, as described in Sec. II B. Vibrational free energies G_{vib}, zero-point energies ZPE, and vibrational entropies S_{vib} were calculated using single-atom displacements with 0.02 Å displacement steps taken in both directions along the lattice vectors for the topmost nine Pt atoms. If any imaginary, or unstable, vibrational modes were found during through this vibrational analysis, these modes were not taken into account. These vibrational modes are unphysical for stable configurations. Moreover, if further convergence results in real vibrational modes, these are likely weak and their contribution to the overall vibrational energy is sensitive to computational errors.

From the above calculations, we derive the formation energy of all relevant individual configurations containing n H atoms per simulation cell, corresponding to the following chemical reaction:

$$Pt_{surf} + \frac{n}{2}H_2(g) \rightarrow Pt_{surf}H_n, \tag{1}$$

as defined in the following equation:

$$\Delta G_{n,conf} = E_{DFT} + \Delta G_{vib,n,conf} - E_{Pt(111)} - \frac{n}{2}\Delta G_{H_2}. \tag{2}$$

Here, ΔG_{H_2} is the formation energy of molecular hydrogen and $E_{Pt(111)}$ is the DFT energy calculated for the Pt slab. Note that the definition of $\Delta G_{vib,n,conf}$ depends on the structure of platinum

hydride in question. If the Pt(111) surface is not distorted or displaced significantly and H only adsorbs on top of the surface, $\Delta G_{\text{vib},n,\text{conf}}$ only depends on the vibrational modes of the H atoms, as in the following equation:

$$\Delta G_{\text{vib},n,\text{conf}}\big|_{\text{on-surface}} = G_{\text{vib},n,\text{conf}}\big|_{\{H\}}. \tag{3}$$

However, if the hydrogenated Pt surface can no longer be described as a Pt(111) surface with chemisorbed hydrogen at the interface—due to H-induced distortion or subsurface permeation of H—the change in the chemical environment of the top Pt layer atoms compared to the pristine Pt(111) slab means that we have to find the difference between the vibrational modes between H and the affected Pt atoms, on one hand, and the top layer of Pt in the Pt(111) slab, as in the following equation:

$$\Delta G_{\text{vib},n,\text{conf}}\big|_{\text{distorted surface}} = G_{\text{vib},n,\text{conf}}\big|_{\{Pt_{\text{top}},H\}} - G_{\text{vib},\text{Pt}(111)}\big|_{\{Pt_{\text{top}}\}}, \tag{4}$$

with the second, third, and fourth layers of the slab, or rump slab, not being considered. Finally, for the most stable configuration for each n of H atoms, we counted $W_{n,\text{conf}}$: the number of unique configurations, which can be obtained by transforming the initial configuration using the intrinsic symmetries of the Pt(111) slab. This means that they are translated, rotated in-plane by $120°$ or $240°$, or mirrored with respect to the plane perpendicular to the slab surface and including the positions of adjacent Pt atoms in different slab layers. This method for finding chemically equivalent configurations was also used in the work of Arulmozhi *et al.*[23] The resulting configurational entropy contribution is shown as follows:

$$S_{n,\text{conf}} = k_B \ln(W_{n,\text{conf}}). \tag{5}$$

Some configurations can be non-mirror-symmetric with respect to the plane perpendicular to and along the Pt(111) surface bridge sites. Pt(111) is non-mirror-symmetric either in this respect, given that the fcc and hcp hollow sites are chemically different, yet are on opposite sides of any bridge site. This means that the configuration is also probably stable when all atoms not directly binding to the lower Pt layers are mirrored with respect to these bridge sites, yet the resulting configuration is unique and needs to be taken into account. The free energy contribution of this bridge-mirrored configuration depends on the difference in free energy between itself, $\Delta G_{n,\text{mirrconf}}$, and the original configuration. Since the chemical environment for a similarly stable configuration is likely similar as well, we assume that the difference in free energy is approximately equal to the difference in E_{DFT} or $\Delta E_{n,\text{mirr}}$. Hence, we find the bridge-mirror free energy contribution $\Delta G_{n,\text{mirr}}$, as described in the following equation:

$$\Delta G_{n,\text{mirr}} = -k_B T \ln\left(\exp\left(-\frac{\Delta G_{n,\text{mirrconf}}}{k_B T}\right) + \exp\left(-\frac{\Delta G_{n,\text{conf}}}{k_B T}\right)\right) - \Delta G_{n,\text{conf}}$$
$$\approx -k_B T \ln\left(1 + \exp\left(-\frac{\Delta E_{n,\text{mirr}}}{k_B T}\right)\right). \tag{6}$$

Finally, using the free energy of the most stable configuration and the free energy contributions of all relevant symmetry-equivalent and bridge-mirrored configurations, we obtain the free energy of the configuration at 0 V vs RHE,

$$\Delta G_n\big|_{\text{0V}} = \min(\Delta G_{n,\text{conf}}) - TS_{n,\text{conf}} + \Delta G_{n,\text{mirr}}. \tag{7}$$

The corresponding free energies at the electrochemical potential U, i.e., $\Delta G_n\big|_U$, are calculated using the computational hydrogen electrode model,[27]

$$\Delta G_n\big|_U = \Delta G_n\big|_{\text{0V}} + eU. \tag{8}$$

B. Cell-specific parameters and construction

$H_2(g)$ was calculated as a single molecule in an 11 Å cubic unit cell. Calculations were performed at the Γ-point and 10^{-4} eV Gaussian smearing without dipole–dipole corrections. Relaxation is performed using the conjugate gradient (CG) optimization method in VASP. The original slab cell, which represents the platinum surface, contained four 3×3 atom layers of triangularly distributed Pt atoms spaced to have equal interatomic distances to bulk platinum. The corresponding cell was hexagonal, with parameters $a = 8.438$ Å, and $c = 25$ Å. The excess space in the long lattice vector reduces spurious slab–slab interactions, which is further aided by dipole–dipole interaction corrections perpendicular to the slab.[28] The k space was sampled using a Γ-centered $4 \times 4 \times 1$ Monkhorst–Pack grid.[29]

The Pt layers in the slab cell were stacked in an ABCA pattern to form a section of the fcc bulk structure along the (111) facet. From this pristine Pt(111) slab, all on-surface *H configurations (1 and 2 ML) are derived. A schematic illustration of the slab with and without on-surface *H is shown in Figs. 1(a) and 1(b), respectively. The positions of the top two layers of Pt and H atoms were relaxed using the CG method up to a maximal force of 0.05 eV Å^{-1}, while keeping the lower two layers fixed to simulate the underlying bulk metal. From these original slabs, cells with subsurface hydrogen were created by inserting hydrogen atoms between the top layer and the subsurface layer (immediately below the top Pt layer), forming layered platinum hydrides, as described in Fig. 1(c). Other configurations, including many configurations containing more than 2 ML *H, were created by including additional hydrogen atoms between the original H and Pt atoms. Details of the construction of these structures are discussed in Sec. III. Relaxation of these structures required additional steps in order to maintain the desired layered structure. First, all atoms except the top Pt layer and on-surface *H atoms were fixed, while other atoms were relaxed for ten iterations
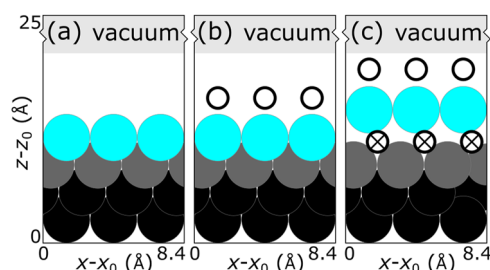
FIG. 1. Global setup of slab simulation cells and configurations. Fixed (bulk) Pt atoms are shown in black, the subsurface (second) Pt layer is shown in gray, and the surface (top) Pt layer is shown in blue; on-surface and subsurface H atoms are shown using blank and crossed white circles, respectively. (a) Clean Pt(111) slab. (b) Pt(111) slab with on-surface H atoms. (c) Pt(111) slab with on-surface and subsurface H.

using the steepest-descent method; subsequently, the same atoms were relaxed up to a force of 0.10 eV Å^{-1} using the CG method. Finally, only the bottom two Pt layers were fixed, allowing the subsurface H and Pt layers to relax along with the top Pt and H atoms using the CG method up to a force of 0.05 eV Å^{-1}.

Coordinates of configurations discussed in Sec. III are included in the supplementary material. All potentials in this work are reported in the RHE scale making use of the computational hydrogen electrode approach[27] such that a comparison with experimental potentials is straightforward. We note, however, that the proton source in acid and alkaline environments is different: H_3O^+ and H_2O, respectively, which may introduce different kinetic behaviors as a function of pH. This cannot be captured by the computational hydrogen electrode as it is merely a thermodynamic approach.

III. RESULTS

A. Pre-1 ML H

Several configurations were tested in which one hydrogen atom was deposited above the topmost layer of Pt atoms in various symmetry-inequivalent configurations and one hydrogen atom was inserted in the subsurface. In all cases, the binding energy of subsurface H was significantly less favorable than its on-surface equivalent. In fact, the optimum configuration suggests an onset potential of −0.50 V vs RHE, as opposed to the predicted onset potential of 0.39 V for 2/9 ML on-surface *H formation in the work by Arulmozhi et al.[23] Hence, it is unlikely that subsurface H is observed for coverages smaller than 1 ML. This result is consistent with experimental observations by Stoerzinger et al.[15]

B. 1 and 2 ML H surface hydrides

1. Configurations

1 and 2 ML configurations were created by combining Pt and H layers, as described in Sec. II. These configurations can be subdivided into those containing only on-surface *H and those with subsurface hydrogen. The construction of these configurations will be discussed in Subsections III B 2–III B 4.

2. On-surface

For the on-surface structures, Pt atom positions are taken from the pristine Pt(111) slab. 1 ML *H configurations are constructed by putting nine equidistant H atoms within 2 Å from the first layer Pt atoms while translating the H atoms to lie over the bridge sites between the first layer atoms and the threefold symmetry surface sites above the first, second (hcp sites), and third (fcc sites) Pt layers, as shown in Fig. 2(a). 2 ML *H configurations were constructed by taking on-top, hcp, and fcc-bound 1 ML *H structures and adding 1 ML *H onto the unoccupied top, hcp, or fcc sites as described above. The latter structures are shown in Fig. 2(c).

3. Subsurface

For the subsurface platinum structures, the lower three Pt layers of the Pt(111) slab are used to support the surface platinum hydride, hereafter named the second, third, and fourth layers for the sake of consistency with on-surface *H structure descriptions. Initial subsurface H configurations are made using 1 ML of equidistant H on the twofold symmetric (bridge) sites between the atoms of the underlying (second) Pt layer, on top of the atoms of the second Pt layer, or on the third (hcp) or fourth (fcc) layers of the (rump part of the) slab [Fig. 2(b)]. Subsequently, an additional 1 ML of equidistant Pt atoms is added on top of the aforementioned H atoms, either between the atoms of the second layer or directly above the atoms of the second layer, the atoms of the third layer, or the atoms of the fourth layer [Fig. 2(c)]. Above this first Pt layer, we added 1 ML of equidistant H, offsetting the positions to correspond to the top, bridge, and two hollow sites of the first Pt layer [Fig. 2(d)]. Relaxation of one 2 ML configuration with one additional subsurface hydrogen atom—which will be discussed in Subsection III D—led
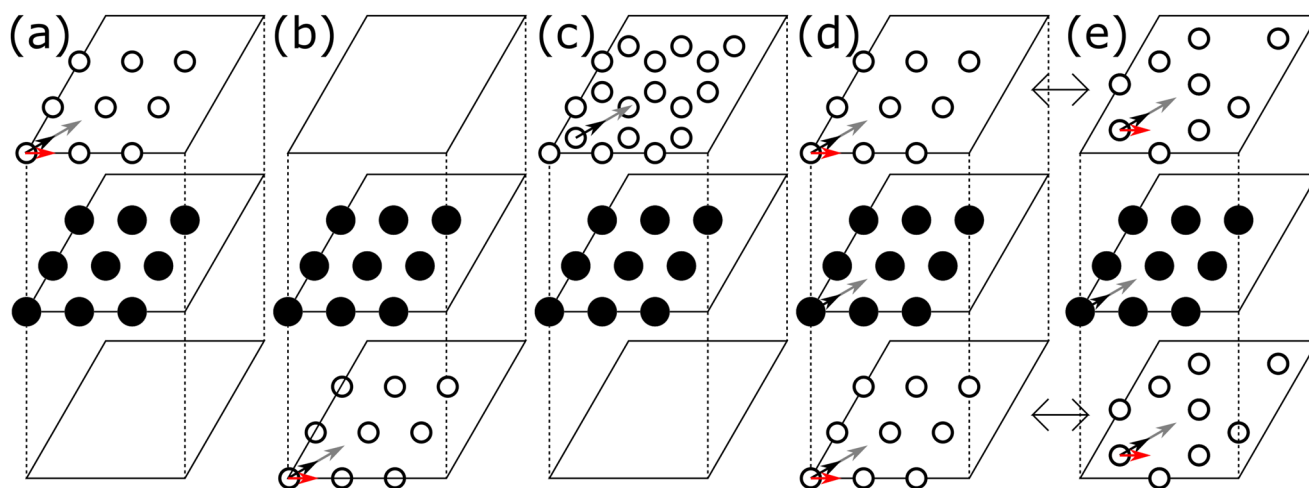
FIG. 2. Construction of 1 and 2 ML H surface platinum hydride configurations. Pt atoms are black solid circles, and H atoms are white circles. Individual layers are represented by planes stacked in the direction of the dotted lines, while arrows indicate possible displacements of the described atomic configurations within their respective layers. (a) 1 ML, on-surface H. (b) 1 ML, subsurface H. (c) 2 ML, on-surface H. 2 ML, on-surface and subsurface H, with equidistant (d) and honeycomb (e) H configurations.

to the formation of a roughly hexagonal configuration of H atoms near bridge sites; after removing the additional hydrogen atom and moving one hydrogen atom to obtain near-$(\sqrt{3} \times \sqrt{3})R30°$ symmetry, one obtains the honeycomb configuration, with a commensurate distortion in the top Pt layer [Fig. 2(e)]. Therefore, we added additional honeycomb H configurations, both on-surface and subsurface, for the 2 ML H configurations and combined them randomly with the other configurations as described above. All 2 ML H configurations are described in Figs. 2(c) and 2(d).

4. Calculated energies

DFT total energies were calculated as discussed in Sec. II. The most stable on-surface configuration for 1 ML H, with H in the fcc hollow sites, is shown in Fig. 3(a). The most stable subsurface configuration for 1 ML H, with H right underneath the Pt atoms in the top layer, is shown in Fig. 3(b).

The calculated energies suggest that subsurface H is significantly less stable than *H when only 1 ML of H is present in the surface, with the energy difference being +4.73 or 0.53 eV per H atom. Hence, it is likely that for near 1 ML H coverages, no significant subsurface adsorption occurs.

The most stable on-surface and on-surface plus subsurface 2 ML H configurations are shown in Figs. 4(a) and 4(b), respectively; the 2 ML H honeycomb configuration is shown in Fig. 4(c).

As opposed to the systems containing 1 ML H, the most stable 2 ML H configuration includes subsurface hydrogen. This subsurface hydrogen binds on top of the second layer Pt atoms, while the first layer of Pt atoms binds on top of the subsurface hydrogen, forming a stacked surface Pt hydride commensurate with the
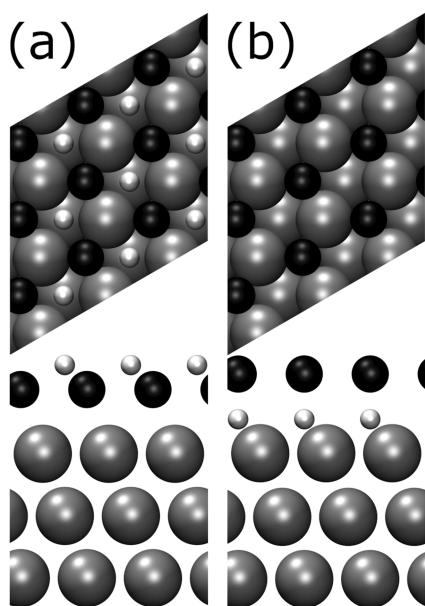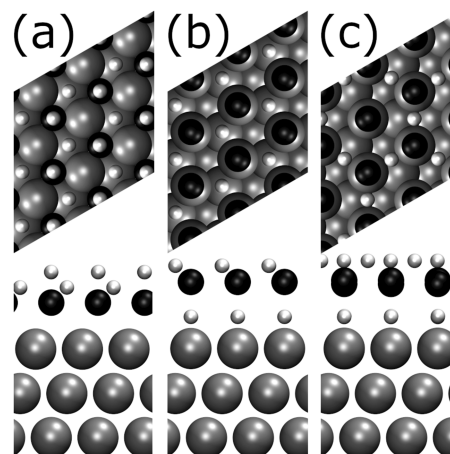
FIG. 4. 2 ML configurations, shown from top (above) and side (below) perspectives. Hydrogen atoms are shown in white, top layer Pt atoms are shown in black, and subsurface Pt atoms are shown in gray. (a) 2 ML on-surface. (b) On-surface plus subsurface, stacked. (c) On-surface plus subsurface, honeycomb. The structure in (b) is 3.83 eV more stable than the structure in (a) and 0.86 eV more stable than the structure in (c).

Pt slab. The resulting topmost layer is covered by 1 ML of equidistant on-surface H directly above the third Pt layer. The competing only-on-surface 2 ML *H configuration in which H is bound to fcc and on-top sites is markedly less stable, with a formation energy of 4.93 eV. Another on-surface plus subsurface stacked configuration [shown in Fig. 4(c)], with an on-surface honeycomb configuration, has a formation energy of 1.99 eV. Hence, the stacked Pt hydride configuration dominates as it has a formation energy of 1.10 eV.

C. >3 ML H platinum hydrides
1. 3 ML H platinum hydrides

3 ML H platinum hydrides were constructed by adding 1 ML H to all unrelaxed 2 ML configurations. More specifically, one set of initial 3 ML configurations has 1 ML H in subsurface sites and 2 ML H on-surface. In these structures, subsurface H is placed onto the second Pt layer bridge, top, hcp, and fcc sites, and on-surface H is adsorbed onto any two of the set of top, hcp, and fcc sites. The positions of the subsurface H layer and the on-surface H layers are similar to those included in the initial 2 ML configurations. The other set of initial configurations contains the 1 ML H on-surface and 2 ML H subsurface; since these structures require the subsurface to accommodate one additional monolayer of H, we have used the energetically favored stacked 2 ML H structure and adsorbed 9 H atoms between the spaces left between the first Pt layer and the subsurface H layer, on the one hand, and the subsurface H layer and the second Pt layer, on the other hand. A final set of configurations is formed by elevating successive rows of first-layer Pt atoms relative to the surface and each other while inserting H atoms on and below the alternating triangular sites between the elevated atoms; the remaining H atoms are placed above the lowermost and uppermost Pt atoms. The schematic structures of these initial configurations are illustrated in Fig. 5. Apart from these configurations, platinum

FIG. 3. Most stable 1 ML configurations. Hydrogen atoms are shown in white, top layer Pt atoms are shown in black, and subsurface Pt atoms are shown in gray. (a) On-surface. (b) Subsurface. The structure in (a) is 4.73 eV (0.53 eV/H atom) more stable than the structure in (b).
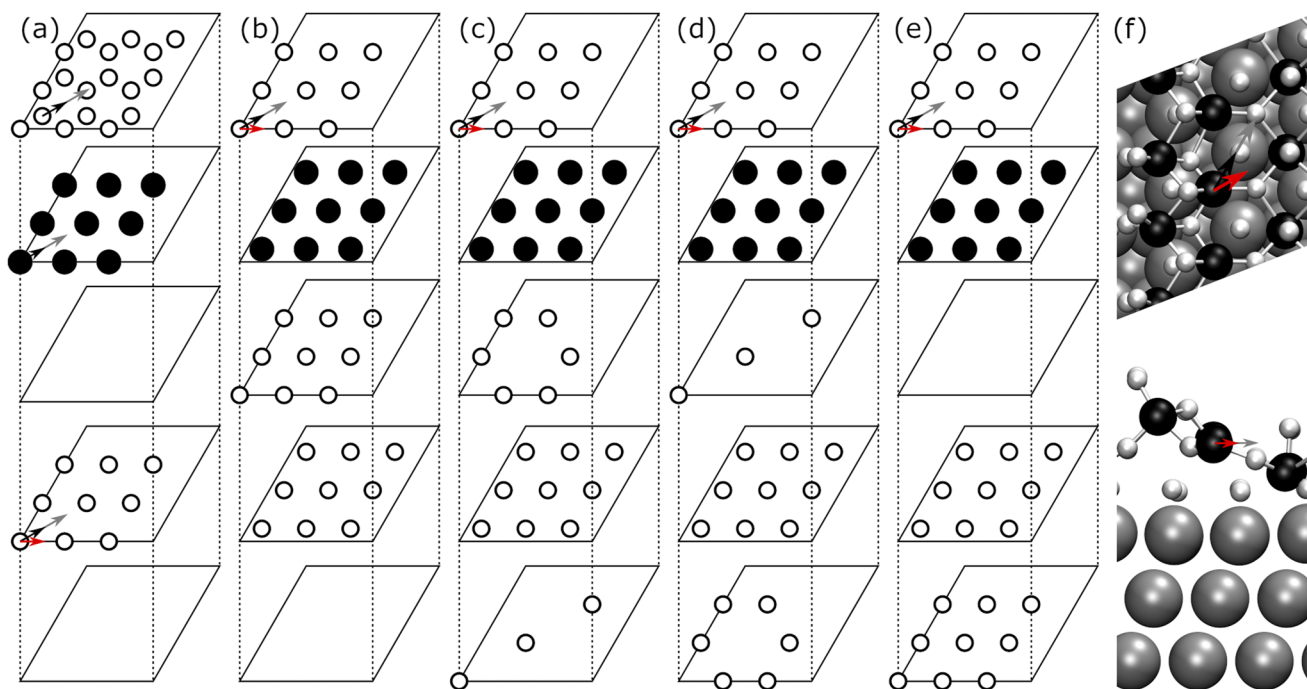
FIG. 5. Construction of 3 ML H surface platinum hydride configurations. Pt atoms are black solid circles, and H atoms are white circles. In (a)–(e), individual layers are represented by planes stacked in the direction of the dotted lines, while (f) shows a top (above) and side (below) view of an initial configuration in which subsurface Pt is represented by larger gray spheres. Arrows indicate possible displacements of the described atomic configurations within their respective layers. (a) 2 ML on-surface and 1 ML subsurface H. 1 ML on-surface H, 1 ML subsurface H, with (b) 1 ML H between first-layer Pt and subsurface H, (c) 2/3 ML H between first layer Pt and subsurface H and 1/3 ML H between second-layer Pt and subsurface H, (d) 1/3 ML H between first-layer Pt and subsurface H and 2/3 ML H between second-layer Pt and subsurface H, and (e) 1 ML H between second-layer Pt and subsurface H. (f) Tilted PtH$_2$ slab on 1 ML subsurface H.

hydride systems containing 3 ML of subsurface H were explored, more specifically in the original subsurface H of the stacked configurations and the two vacant zones described above; these structures detached from the second and lower Pt layers spontaneously during relaxation.

One specific configuration, with a tilted PtH$_2$ slab adsorbed onto the bridge sites between subsurface H atoms, as shown in Fig. 5, formed a disordered surface structure after relaxation. In this structure, the top Pt layer is split into two sublayers, with part of the on-surface H inserted itself between the Pt atoms nearer and further from the second Pt layer, and the lower Pt atoms stacked on top of the subsurface H atoms. The structure is further optimized by shifting the two sublayers and the 18 topmost H atoms by half a bulk Pt–Pt distance along one of the surface lattice vectors. Subsequent relaxation of the structure causes the nine Pt atoms to further separate into three sublayers, with a row of three Pt atoms suspended by two Pt atoms, on one side, and one, on the other, which are in turn supported by three Pt atoms stacked on top of the subsurface H atoms and the second Pt layer. These Pt atoms are each surrounded by n H atoms, or n-coordinated by H, for $n = 4$–6. Except for the single Pt atom in the middle sublayer, which is four-coordinated by H in a roughly planar structure, all topmost Pt atoms are six-coordinated by H—in an octahedral structure, occasionally distorted to accommodate for the other surface atoms—or five-coordinated in a square-pyramidal fashion. Moreover, the topmost row of Pt atoms

does not bind directly to the subsurface stacking layer of H, binding through at least two successive H atoms. The stable 3 ML H platinum hydride structure is shown in Fig. 6.

The original stacked structures are generally stable without vibrational corrections, with a formation energy of 5.90 eV. However, the three-dimensional structure shown in Fig. 6 is significantly more stable with a formation energy of 4.33 eV (1.57 eV more stable). This suggests an onset potential more negative than −0.11 V relative to the most stable 2 ML H configuration.

2. 4 ML platinum hydrides

4 ML configurations were formed by adding nine H atoms to the most stable (three-dimensional) 3 ML H platinum hydride structure displayed in Fig. 6. First, single H atoms were added near the topmost nine Pt atoms, in such a way that either the six-coordination of the individual atoms is maintained or additional H atoms are added to the four-coordinated Pt atoms, above and below the plane in its coordination shell. If necessary, H atoms were moved around to maintain distances greater than 1.2 Å between them—roughly halfway between the H–H distance in H$_2$(g) (~0.7 Å) and the typical Pt–H distances (~1.5–2.0 Å). Next, these template configurations were combined by adding the hydrogen atoms not originally included in the 3 ML structure and moving the other atoms corresponding to the individual templates. If one atom is displaced relative to the 3 ML structure in multiple templates, the average
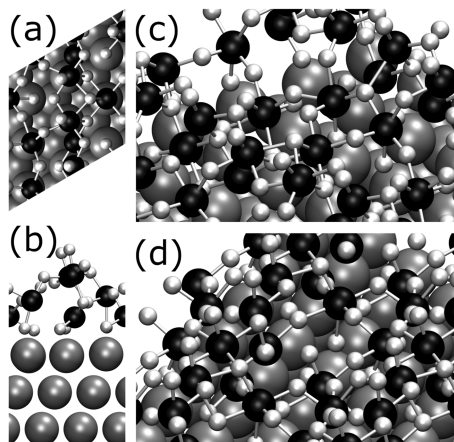
FIG. 6. Three-dimensional 3 ML H platinum hydride structures. Hydrogen atoms are shown in white, top layer Pt atoms are shown in black, and subsurface Pt atoms are shown in gray. (a) Top view. (b) Side view parallel to top sublayer rows. (c) and (d) Alternate angle views.

displacement is used. Finally, structures in which all interatomic distances are greater than 1.2 Å were selected for relaxation.

In all the resulting 4 ML H configurations, except for one, relaxation resulted in one or multiple pairs of H atoms moving together to less than 1.0 Å and in some cases moving away (>2 Å) from the surface. Since these structures cannot be considered to contain chemisorbed or Pt-bound atomic hydrogen, these structures were rejected. The remaining 4 ML H structure, which appears more disordered than the 3 ML H structures, yet is metastable, is shown in Fig. 7. This structure contains many of the surface features of the three-dimensional 3 ML H structure, with multiple five-coordinated and six-coordinated Pt atoms. Contrary to the 3 ML H platinum hydride, two hydrogen atoms in the stable
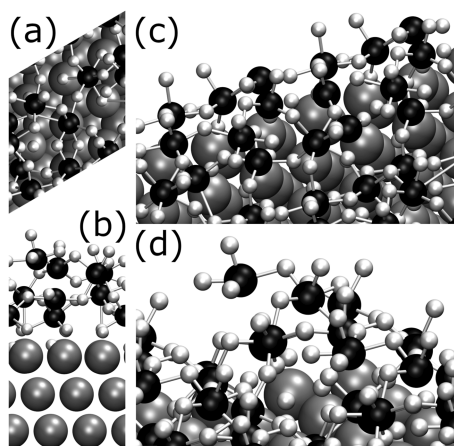
FIG. 7. 4 ML H platinum hydride structures. Hydrogen atoms are shown in white, top layer Pt atoms are shown in black, and subsurface Pt atoms shown in gray. (a) Top view. (b) Side view parallel to top sublayer rows. (c) and (d) Alternate angle views.

4 ML H configuration bind directly to the second Pt layer, beneath the other subsurface H atoms. Moreover, five of the first-layer Pt atoms do not bind directly to subsurface H, with one five-coordinated Pt atom binding to the slab through at least three successive H atoms. The formation energy of this 4 ML H configuration is 8.30 eV.

D. Interstitial configurations

Configurations were created by adding or removing single H atoms from the several integer ML configurations constructed as described above, either before or after relaxation, to assess whether the integer ML structures form islands of stability, i.e., H binds more favorably than in all studied configurations with similar but lower or higher H coverages.

1. 1 ML ± 1 H

For 1 ML *H on Pt(111), the thermodynamic effects of removing an atom have been thoroughly described in the work of Arulmozhi *et al.*:[23] the binding energy of the additional atom is −0.06 eV. 1 ML + 1 H (technically 1 1/9 ML H); configurations are obtained by taking all possible equidistant 1 ML H configurations on-surface and subsurface, while subsequently adding single hydrogen atoms. Adding one additional H atom onto an on-top site of the Pt(111) slab with 1 ML on fcc sites, which is the most stable configuration for 1 ML + 1 H, incurs a free-energy penalty of +0.42 eV. Therefore, this is expected to only occur for negative potentials vs RHE.

2. 2 ML ± 1 H

Configurations were created by adding or removing single H atoms from either the stacked or the entire set of 2 ML configurations described above, respectively. Single H atoms in both symmetry-inequivalent sites (on-surface and subsurface) were removed from this stacked 2 ML H platinum hydride to form 2 ML − 1 H configuration (essentially 1 8/9 ML) hydrides. Additionally, single H atoms are added to all initial 2 ML H platinum hydrides in the vacant sites to find the most stable 2 ML + 1 H configuration (2 1/9 ML H).

The most stable structure of the 2 ML − 1 H platinum hydride corresponds to the stacked structure, albeit with one on-surface H atom removed. The binding energy of this final surface H atom needed to form 2 ML is −0.46 eV, to be compared to the formation energy of 2 ML H platinum hydride from 1 ML on-surface *H on Pt(111), which is +0.30 eV/atom. In contrast, the most stable structure of the 2 ML + 1 H platinum hydride has one additional H atom on an fcc site of the second Pt layer, which is directly above a fourth Pt layer atom. The binding energy cost of the additional H atom is +0.73 eV, which is significantly more positive than the binding energy of the previous H atom.

3. 3 ML − 1 H

Structures were constructed by removing single symmetry-inequivalent H atoms from the initial (unrelaxed) stacked 3 ML H platinum hydrides and by removing single symmetry-inequivalent H atoms from the three-dimensional 3 ML H platinum hydride. One configuration was specifically favored in which the H atom between the 2 Pt atom clusters, in the middle Pt sublayer of the surface hydride, is absent. The binding energy of this additional hydrogen

atom is +0.30 eV, which is again smaller than the energy difference per atom between 2 and 3 ML H (+0.36 eV/atom).

All data discussed above are summarized in Fig. 8. We observe that the 2 ML H configuration specifically forms an island of stability: it is favorable to form it from an H coverage slightly below 2 ML, the next H atom binds very poorly compared to H adsorption at other coverages, in general, and even the overall binding energy of H atoms is improved with respect to the adjacent coverages. Compare this to hydrogen adsorption on Pt(111) as discussed in the work of Arulmozhi *et al.*, for which there is no such zone of stability.[23] 3 ML H is possibly an island of stability as well: although H does not bind more strongly than in 3 ML − 1 H, forming the 3 ML H structure from 3 ML − 1 H is more favorable than forming the latter from 2 ML H + 1 H. Conversely, 1 ML H does *not* appear to be a local minimum, neither when it comes to overall H binding energy nor in reduction potential. One should mind that the optimum configurations described above might not be the global minima for their respective H coverages. The possible consequences of using suboptimal configurations toward (relative) formation energies will be exposed in Sec. IV.

E. Thermodynamics and hydride stability

1. Vibrational analysis, configurational entropies, and Gibbs free energies

The locally stable configurations, obtained as described in the individual configuration Subsections III C and III D, were sampled
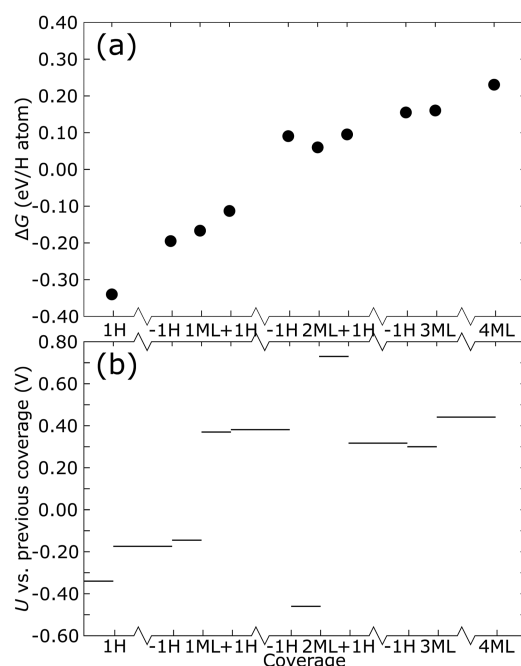
FIG. 8. Binding energies of H atoms for various H coverages on Pt(111) and in Pt surface hydrides. (a) Binding energies per H for all H atoms. (b) Average binding energies of 1 or 8 H atoms relative to the adjacent lower-coverage hydride configuration.

to obtain all possible globally stable configurations sufficiently different when assessed according to specific properties. While sampling the configurations, we considered that the forces exerted during distortion of the lattice—and hence the vibrational mode excitation energies—depend on the chemical environment of each atom, which we assume to be predominantly affected by the number of nearby atoms of any species and the local symmetry. Hence, our criteria were whether the top Pt layer is distorted by H insertion or not, the stacking pattern of H and Pt layers, and the approximate translational symmetry of platinum hydride. The energetically most favorable configuration per set of criteria and H coverage is used for further analysis; within each H coverage, we selected all systems that have internal energies no more than 0.15 eV/H atom above the configuration with the lowest internal energy to ensure that one within the set has the most stable configuration overall. Again, for each H coverage, we calculated the vibrational free energies for these configurations, starting with the most negative DFT energy and moving toward less energetically favored configurations, until the current configuration has a more positive DFT energy than the total Gibbs free energy for the most stable configuration up to that point. The DFT and vibrational energies of these structures are shown in Table I.

For each of the most stable configurations, the configurational entropy was calculated. The 1 ML H configuration is 1×1 periodic, which means no other chemically equivalent configuration can be obtained; hence, its configurational entropy is zero. When one H atom is added to this structure, the atom can be positioned on any out of 3×3 top sites, which means that there are nine equivalent configurations: $W_{conf} = 9$. The 2 ML H configuration is 1×1 periodic, similar to the 1 ML H structure; hence, $TS_{conf} = 0$. Similar to adding one H atom to 1 ML, adding 1 H atom to or removing 1 H atom from the stacked 2 ML H structure increases the number of equivalent configurations to $W_{conf} = 9$. Contrary to the more highly periodic configurations above, the 3 ML − 1 H, 3 ML H, and 4 ML H structures can be freely translated and rotated across the surface, generating $W_{conf} = 27$ unique symmetry-equivalent configurations.

For all configurations suspended by a monolayer of "stacked" H atoms, we took into account bridge-mirrored configurations. For 2 ML − 1 H, 2 ML H, and 2 ML + 1 H coverages, the energy differences amount to 0.004 eV for each, contributing −0.02 eV to their overall free energies. However, the mirrored configurations for the 3 ML − 1 H and 3 ML H structures are 0.06 eV less stable. Since the configurations only contribute significantly (0.005 eV or more) to the free energy of the corresponding coverage if they are within 0.04 eV of the most stable structure, these mirrored configurations do not affect the overall free energy for their H coverages.

For the 4 ML H configuration, E_{DFT} of the bridge-mirrored configuration is 0.29 eV lower than the energy calculated for the original configuration obtained above. Otherwise, the coordination of Pt and H atoms follows the same pattern as the original 4 ML H configuration. This bridge-mirrored configuration is used to calculate charges and the overall free energy and is shown in Fig. 9.

The thermodynamically optimum configurations correspond to those that were found to have the most negative DFT energies, and they have been described in Subsections III C and III D.

TABLE I. Free energies of individual nH configurations. Numbers printed in boldface correspond to the most stable configuration for its specific H coverage.

Coverage	Configuration[a] $\Delta G_{str} - \Delta G_{vib}$ (eV)	ΔG_{vib} (eV)	ΔG_{str} (eV)	TS_{conf}	ΔG_{mirr}	ΔG (eV)
1 H	−0.43	0.14[b]	**−0.28**	0.06	0.00	**−0.34**
	0.38	0.13	0.56	0.06		
1 ML	−2.87	1.37[b]	**−1.50**	0.00	0.00	**−1.50**
	2.49	0.74	3.24	0.00		
1 ML + 1 H	−2.65	1.57	**−1.08**	0.06	0.00	**−1.13**
	−2.47	1.53	−0.94	0.06		
2 ML − 1 H	−1.13	2.75	**1.61**	0.07	0.02	**1.54**
	−0.83	2.74	1.91	0.07		
2 ML	−1.27	2.37	**1.10**	0.00	0.02	**1.08**
	−0.83	2.82	1.99	0.03		
	1.57	2.79	4.93	0.00		
2 ML + 1 H	−1.12	3.15	**2.03**	0.07	0.02	**1.81**
	−0.82	3.00	2.18	0.07		
	−0.73	3.02	2.29	0.07		
	−0.69	3.02	2.33	0.07		
3 ML − 1 H	−0.35	4.68	**4.11**	0.09	0.00	**4.03**
	0.74	4.46	5.20	0.09		
	0.84	4.46	5.30	0.09		
	0.92	4.37	5.29	0.09		
	0.99	4.60	5.59	0.09		
3 ML	−0.27	4.68	**4.41**	0.09	0.00	**4.33**
	0.69	4.55	5.23	0.09		
	1.29	4.64	5.93	0.03		
4 ML	1.80	6.59	**8.39**	0.09	0.00	**8.30**
	2.06	6.57	8.63	0.09		

[a]Each line represents a single configuration, which is potentially stable for the specific H coverage.
[b]Vibrational energies based on H atoms only, as defined in Sec. II A.

2. Pt–Pt interatomic distances

The distances between surface (hydrogenated) Pt atoms individually and between surface Pt atoms and subsurface Pt atoms generally increase with the increasing H coverage, as shown in Fig. S1. Simultaneously, the shortest Pt–Pt distances for each surface Pt atom remain constant or decrease slightly for the increasing H coverage. Both effects are analogous to the displacement of Pt atoms in PtH-II by intercalating H layers relative to bulk Pt, as observed by Scheler *et al.*[12] Contrary to bulk hydride PtH-II, the surface hydride is exposed to vacuum. This allows for larger Pt–Pt spacing and greater disorder, the latter to the extent that surface Pt atoms in some high-coverage configurations are closer to subsurface Pt atoms than to the surface. All the above H coverage and vacuum interface effects are clearest for the more stable structures, suggesting that Pt displacement and some degree of (in-layer) disorder are necessary for obtaining an optimum hydride configuration on Pt(111).

3. Relative stabilities and onset potentials

Using the Gibbs free energies, we can calculate the relative stabilities of the various surface Pt hydrides. The energy–potential diagram stability diagram is shown in Fig. 10.

From these stability diagrams, we observe that multi-H-layer configurations are thermodynamically stable from an applied electrochemical potential more negative than −0.29 V (vs RHE), at which 2 ML H coverage is favored. This is followed by the adsorption of another full monolayer of H at −0.36 V, forming a 3 ML H platinum surface hydride. Finally, at a potential more negative than −0.44 V, 4 ML surface hydrides are predicted to be formed. However, this is a lower bound since only one configuration could be found for which all H atoms are chemisorbed. Importantly, from the lowermost lines in Fig. 10, we can deduce that there is no electrochemical potential at which any of the interstitial, or non-integer-number ML H, coverages are predicted to be more thermodynamically favored than any of the integer-number ML H
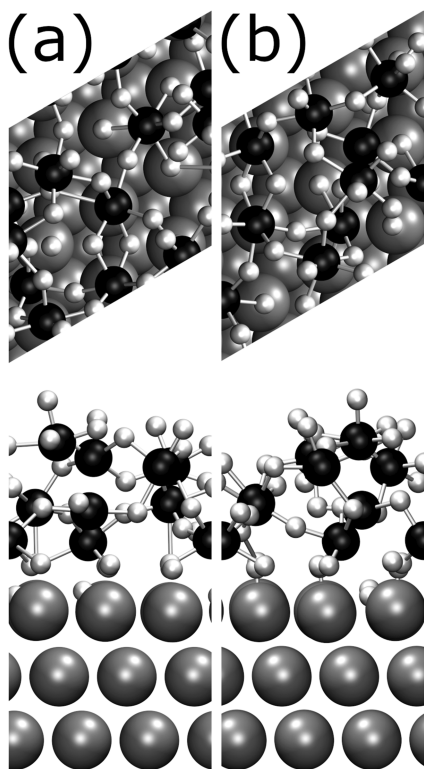
FIG. 9. Original and new bridge-mirrored stable configuration for 4 ML H surface platinum hydride. Hydrogen atoms are shown in white, top layer Pt atoms are shown in black, and subsurface Pt atoms are shown in gray. (a) Original configuration. (b) Bridge-mirrored configuration.
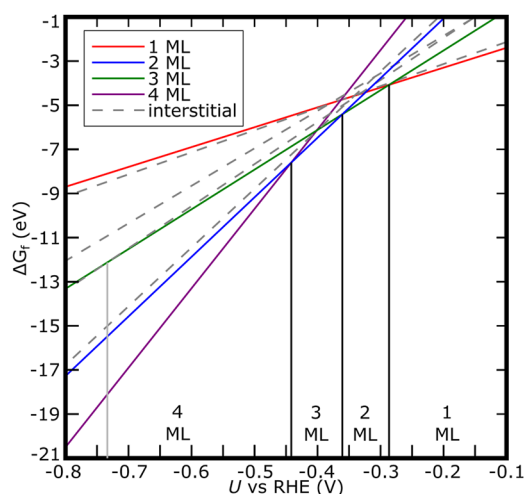
FIG. 10. Stability diagram for surface platinum hydrides. In the energy–potential diagram, solid and dotted lines represent integer and non-integer numbers of H monolayers, while vertical lines represent important transitions and (for the red line) the highest onset potential that is relevant to the overall reduction mechanism.

coverages. One interstitial coverage in which one H atom is added to the 2 ML H platinum surface hydride has a formation onset potential of −0.73 V. The thermodynamic barriers resulting from interstitial coverages, in general, will be discussed later in this paper.

4. Charge calculations

For the most stable structures for each coverage, charges were calculated using the Bader charge method as implemented by Tang *et al.*[30] The corresponding charges are shown in Fig. 11, and the charges assigned to specific sets of atoms are listed in Table II.

A summary of the various correlations and linear relations between the coverages and cumulative charges is listed in Table SI of the supplementary material. There is no clear correlation between the charge in the lowest layer and the overall H coverage, which
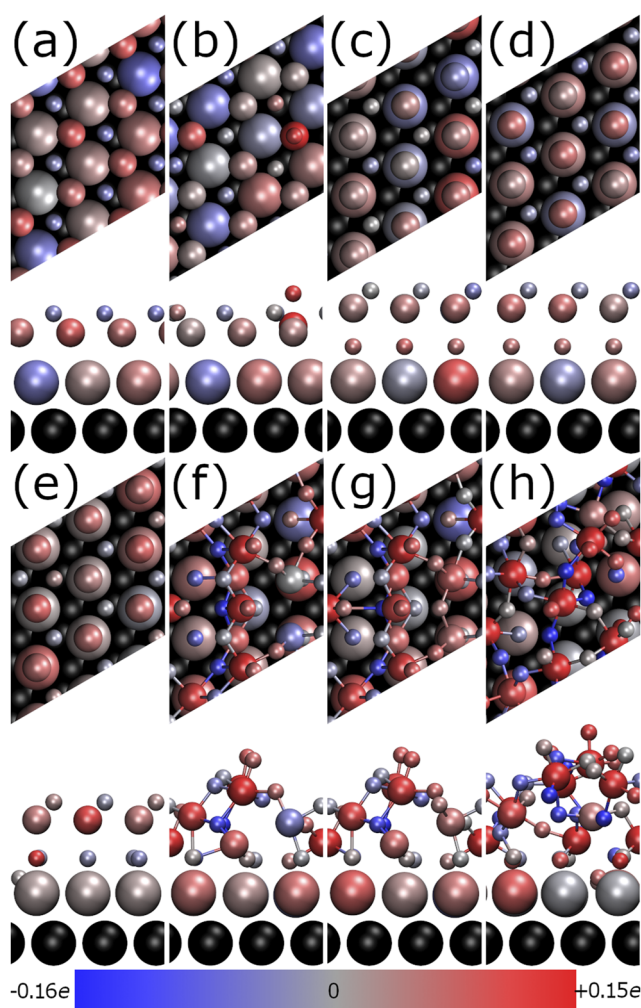
FIG. 11. Charges for stable configurations of various H coverages. H atoms, first layer Pt atoms, and second layer Pt atoms are small, medium-sized, and large, respectively. Charges are represented by blue (negative) through gray (neutral) to red (positive) colors, as described in the bottom. Third- and fourth-layer Pt atoms are black. (a) 1 ML H, (b) 1 ML + 1 H, (c) 2 ML − 1 H, (d) 2 ML, (e) 2 ML + 1 H, (f) 3 ML − 1 H, (g) 3 ML, and (h) 4 ML.

TABLE II. Cumulative charges for specific sets of atoms within platinum hydrides.

	Cumulative charges (e)					
Coverages	First layer Pt	Second layer Pt	Third layer Pt	Fourth layer Pt	Pt → H transfer	Additional H[a]
0 ML[b]	−0.427	+0.439	+0.431	−0.443	⋯	⋯
1 ML	+0.269	−0.023	+0.380	−0.367	−0.259	⋯
1 ML + 1	+0.149	−0.123	+0.382	−0.369	−0.039	+0.057
2 ML − 1	+0.052	+0.006	+0.165	−0.332	+0.110	⋯
2 ML	+0.171	+0.006	+0.173	−0.331	−0.019	−0.018
2 ML + 1	+0.035	+0.003	+0.111	−0.324	+0.175	+0.006
3 ML − 1	+0.402	+0.079	+0.130	−0.352	−0.260	⋯
3 ML	+0.470	+0.043	+0.138	−0.351	−0.300	+0.013
4 ML	+0.778	+0.033	+0.020	−0.342	−0.489	⋯

[a]Charges on an atom in the n ML H configurations removed to obtain the n ML − 1 H configuration or charge on an atom in n ML + 1 H configurations added to the n ML H configuration.
[b]Included for reference.

means that charge is largely transferred from the surface Pt atoms to hydride. The observation of a net negative charge on the lowest (fourth) layer and the topmost (first) layer is possibly caused by artifacts of the Bader charge calculation method on pristine surfaces. In fact, in the 0 ML H pristine reference slab, there is some significant (~−0.427e) charge transfer from the inner layers to the top surface layer, which largely disappears when 1 ML or more H are added to the surface. The charge of the second Pt layer is only weakly dependent on the number of H atoms for all non-zero H coverages. Conversely, the net charges on the third Pt layer and the overall H coverage appear to be anticorrelated (−0.014 e/H, $R = -0.93$), which suggests a transfer of electrons toward the deeper-lying parts of the surface during H adsorption. Similarly, charge transfer from Pt to H is anticorrelated with the charge of the first layer, with −0.86e transferred on average from Pt to H per 1e^- of net first layer charge ($R = -0.95$). However, neither this charge transfer ($R = -0.58$) nor the charge of the first Pt layer ($R = 0.79$) seems to be correlated with the hydrogen coverage. Excluding the 4 ML H configuration decreases these correlation coefficients to $R = -0.26$ and 0.54, respectively.

There is a net (negative) charge transfer from Pt to H for 1 ML H. For 2 ML H, however, H binds neutrally. More specifically, subsurface H is charged positively and on-surface H is charged more negatively although individual atomic charges are ~0.02e. Moreover, removing or adding one H atom with respect to the 2 ML configuration causes net electron transfer toward the Pt slab. For 3 and 4 ML H, the topmost Pt and H atoms are charged positively (~0.07e for 3 ML, 0.12e for 4 ML H), while the highly coordinated H atoms adjacent to the topmost Pt atoms are charged negatively, with charges up to −0.11 and −0.26e for 3 and 4 ML H, respectively.

IV. DISCUSSION

A. Phase changes, local stability, and the nature of integer monolayer platinum hydrides

When increasing the hydrogen coverage from 1 to 2 ML H, the binding of each individual hydrogen atom is more favorable on-surface near 1 ML H, yet is more favorable subsurface near 2 ML H. Simultaneously, the onset potential for the single H atom reduction steps shifts from highly disfavored to highly favored, as illustrated in Fig. 10: from −0.36 V vs RHE for the reduction of 1 ML H to 1 ML + 1 H to +0.47 V vs RHE for the reduction of 2 ML − 1 H to 2 ML H. This change in binding behavior is accompanied by a collective shift of the first Pt layer and subsurface H atoms from their original positions relative to the Pt bulk. This suggests that an important change takes place in the surface, both with respect to the surface structure and with respect to H binding energies, which was not considered by Hong et al. and Légaré.[16,17] Note that Hong et al. found significantly more favorable binding energies overall, including for subsurface hydrogen,[16] but regarded these binding energies as being less reliable due to their usage of (severely overbinding) local-density approximation (LDA) functionals.[31] A perhaps more significant structural change occurs between 2 and 3 ML H: hydrogen first adsorbs below the first layer, but at a certain H coverage between 2 1/9 and 2 8/9 ML, the Pt surface is rearranged and H inserts itself between the first-layer Pt atoms. A similar restructuring of the local Pt structure was observed by Mager-Maury at $Pt_{13}H_n$, with a transition from a biplanar structure with closely bound Pt atoms for $n < 20$ to a more spaced cuboctahedral structure for $n \geq 20$.[18] The final H atom is adsorbed into the surface-facing part of the three-dimensional 3 ML H platinum surface hydrides. For this atom, the H adsorption potential changes from −0.73 to −0.30 V vs RHE.

It is by a large margin more favorable to form the 2 ML H platinum hydride structure by adding one single H atom to the 1 8/9 ML H configuration than it is to add one H atom to this 2 ML H structure. As discussed above, the 2 ML H coverage forms a zone of stability across a large range of electrochemical potentials. This is in contrast to those configurations with *H coverages <1 ML, for which the *H coverage increases gradually with the applied potential (as discussed in-depth in the work by Arulmozhi et al).[23] The relative windows of the stability of 1, 2, and 3 ML H platinum hydride configurations are illustrated in Fig. 12.
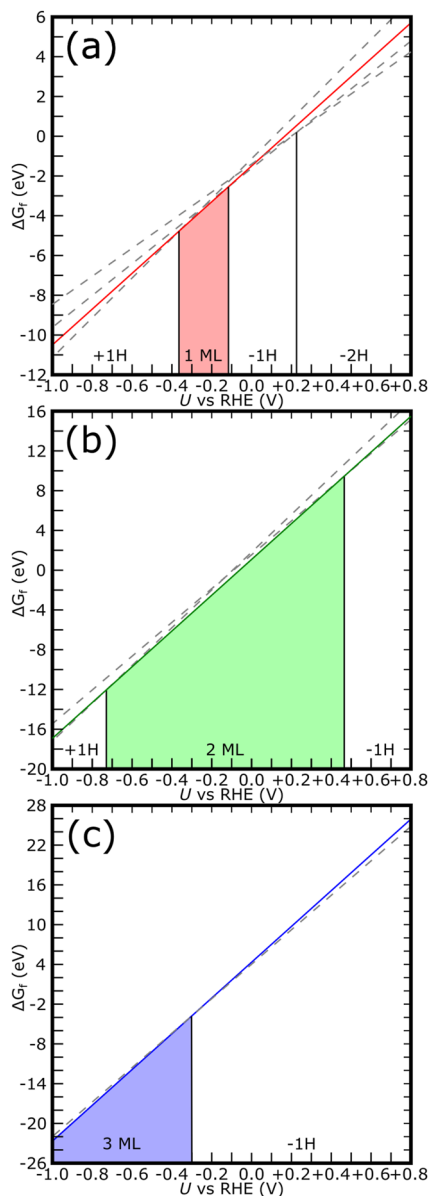
FIG. 12. Relative potential windows of the stability of 1, and 3 ML H coverages with respect to adjacent (±1 H) coverages; 1 ML − 2 H (included for reference) and 1 ML − 1 H energies are taken from the work of Arulmozhi *et al.*[23] (a) 1 ML H vs 1 ML ± 1 H. (b) 2 ML H vs 2 ML ± 1 H. (c) 3 ML H vs 3 ML − 1 H.

The differences between 1, 3, and 4 ML H platinum hydrides, on the one hand, and the 2 ML H platinum hydride, on the other hand, together with the broad potential range of the stability of the 2 ML H platinum hydride, coincide with the binding properties of H for these specific configurations. A net negative charge is transferred to the H atoms, with large Pt–H distances, when they are adsorbed on-surface in a 1 ML *H configuration. In the 3 and 4 ML H structures, H atoms are negatively charged with shorter Pt–H distances with displaced Pt atoms charged positively.

This suggests that rather ionic interactions exist within surface-bound [PtH$_n$] complexes, which implies a stronger hydride character. The only configuration for which no net charge is transferred to H is the stacked 2 ML H configuration: the Pt–H interactions appear to be covalent rather than ionic and could be considered a platinum-hydrogen compound as opposed to a proper platinum hydride. This transition from covalent to ionic binding coincides with an increasingly positive charge on the H atoms when adding hydrogen to 1 ML H to form 2 ML H and an increasingly negative charge on the H atoms when moving from 2 to 4 ML H platinum hydrides. There is a main exception: H in the 2 ML H platinum–hydrogen structure is neutrally charged, while both adding and removing one H atom cause the net charge on H to increase by +0.1 to +0.2e. This does not occur (to this extent) on 1 or 3 ML and, combined with the general tendency of H to bind negatively, may be related to the relative stability of 2 ML across a broad range of applied potentials.

B. Definition of the onset potential

The DFT calculations presented above predict a candidate precursor for cathodic corrosion, namely, the three-dimensional 3 ML H platinum surface hydride, which forms at −0.37 V vs RHE. Cathodic corrosion on Pt(111) has been observed to occur at potentials more negative than −0.5 V vs RHE in alkaline media and requires strongly negative potentials up to −1.0 V vs NHE for significant surface roughening to occur within a reasonable time-frame.[5] However, the kinetics of the reduction mechanisms between the integer monolayer H configurations may also play an important role. The immediate formation of 2 ML H platinum surface hydride from 1 ML *H on Pt(111), accompanied by mass displacement of Pt atoms, is expected to be kinetically slow. This also holds for the formation of 3 ML H from 2 ML H platinum hydride.

Nonetheless, there is also a possible thermodynamic (electrochemical) barrier associated with the metastability of the 2 ML structure, as can be seen in Fig. 12. Adding 1 H to the optimum 2 ML structure has an onset potential of −0.73 V vs RHE, which is not only more negative than the applied potential needed for 3 or 4 ML platinum surface hydride formation but also in agreement with the very negative potentials necessary for rapid cathodic corrosion. It is likely that the distortion of the Pt layer, observed in the formation of the 3 ML H surface platinum hydride, requires greater H coverages than 2 1/9 ML. Hence, subsurface interatomic repulsion will move the predicted thermodynamic barrier for 3 ML H surface platinum hydride formation even higher. The fact that some degree of cathodic corrosion occurs at potentials for which 3 ML H is predicted to be hampered indicates that there may be an alternative cathodic corrosion process starting from the 2 ML H platinum–hydrogen surface. This process should be more similar to the one proposed by Evazzade *et al.*,[10] and since it will not involve a thermodynamically stable, surface-bound hydride intermediate, the nature of this process is beyond the scope of this study.

C. Limitations of the model used

Calculating the real H coverage at each potential requires relaxing all possible H coverages and their respective configurations

while using a functional that calculates free energies within chemical accuracy for platinum surface hydrides. We used a method for generating initial configurations that is exhaustive within its set of rules and constraints and that is defined to generate a broad range of as dissimilar structures as possible while maintaining order in their Pt and H distributions. Although systematic, this explicitly does not span the entire space of possible platinum hydride configurations. An automated algorithm was considered that may eliminate similar structures, which would likely converge to the same optimum. Similar algorithms have been used for small or constrained clusters.[32–34] Assuming that we are able to define a set of rules that finds all reasonable configurations, which converge to different local optima, the number of possible initial configurations is significantly smaller. However, this means that many thermodynamically unfavorable local optima are found. Although one may steer the algorithm toward favorable local optima using alternative methods, including machine learning, the complexity of the hydride structures requires large numbers of configurations to be relaxed to train the algorithm. Hence, applying global optimization algorithms to our surface platinum hydride systems is not (yet) feasible. Moreover, the set of platinum hydride configurations is still limited by the underlying Pt(111) cell, ignoring candidate structures with incompatible translational order.

Even though not all or none of the configurations may be global minima, we have obtained a first approximation toward high density platinum hydrides made under relatively mild electrochemical conditions. Since their energies are clearly below energies for competing configurations (see Table I), it is likely that there are few configurations with lower energies, and any such configurations are probably close in energy. Moreover, the accuracy of the PBE functional is limited to ~0.10 eV,[35] and our calculated onset potential for 3 ML H platinum hydride formation is ~0.10 V more positive than the onset potential of cathodic corrosion. This proximity of a calculated onset potential to that of a measured electrochemical reaction suggests that our (meta)stable structures are sufficiently close to reality when using the PBE functional although more accurate functionals may allow (and require) us to search for possibly more stable local minima.

The structures calculated in this work do not include alkali metal cations although previous studies from our group and others indicate that alkali metal cations adsorb before the onset of cathodic corrosion on Pt[10,11,36] and other metals, such as Au.[37,38] Since many calculations per platinum hydride structure are required to accurately assess the effect of alkali metal cations on each possible adsorption site, calculating these structures was considered outside the scope of this work. It is possible that alkali metal cations compete with hydride structures, but preferentially adsorb in subsurface sites beyond 1 ML H, leaving on-surface sites for alkali cation adsorption. Moreover, the charge polarization and net (negative) charge of the surface hydrides at higher (3 and 4 ML) H coverages may promote the adsorption of cations from the electrolyte, thereby promoting hydride formation in the presence of cations. The resulting alkali-metal-modified hydride structures may serve as an alternative or subsequent intermediate for cathodic corrosion.

A final limitation of our calculations is that they focus only on Pt(111) since cathodic corrosion is most thoroughly studied on this facet. Pt(100) and Pt(110) will likely allow for hydride formation at less negative applied potentials, and there will be less competition from the HER at moderate overpotentials since those facets bind H more strongly than Pt(111).[39] However, cathodic corrosion on non-(111) facets of Pt is slower than on Pt(111), a key experimental observation for which the current work does not provide an explanation.[40] We expect that the four-to-six-coordinated PtH units form the basis of surface hydride structures at greater coverages although the precise spacing, binding energies, interactions, and configuration of these moieties and subsurface H may be markedly different, as well as possible restructuring different to or beyond that considered for Pt(111). These can be clarified by further research on this topic.

V. CONCLUSION

Energies of various 1, 2, 3, and 4 ML H surface platinum hydrides were calculated using DFT in which the top layer is increasingly saturated with chemisorbed hydrogen. Onset potentials for their formation from pristine Pt(111) were obtained using the computational hydrogen electrode. We find that the binding energies of surface platinum hydrides become thermodynamically favorable at potentials ranging from −0.29 to −0.47 V vs RHE. Among these structures, a three-dimensional structure containing 3 ML of atomic hydrogen was found to be remarkably stable. Through distortion of the topmost Pt layer and insertion of H atoms, six-coordinated Pt hydride moieties are formed near the top of the structure. Since these moieties can potentially be cleaved to form aqueous $[PtH_n]^{m-}$ moieties (experimentally known to need stabilization by electrolyte cations for actual dissolution to occur),[11] this 3 ML H structure is a candidate precursor for cathodic corrosion of Pt(111). In fact, the associated onset potential agrees with the negative potentials observed experimentally for cathodic corrosion, especially considering the precision of the computational methods. However, the difficulty in adding additional hydrogen to the 2 ML H surface platinum hydride shifts the effective onset potential to −0.78 V vs RHE. This value is significantly closer to the typical electrochemical potentials at which cathodic corrosion takes place, yet still allows for the formation of high-density Pt hydrides needed as its precursor.

Altogether, the research presented in this work provides insights into the elusive nature of the surface-bound precursor to cathodic corrosion on Pt(111). Future research may provide more information on the thermodynamics and kinetics of the various platinum hydride phase transitions discussed here, including optimum configurations by means of, e.g., global optimization algorithms. More knowledge on the kinetics and mechanism of hydrogen diffusion into the Pt(111) surface during various phases of surface hydride formation, the nature of the HER coinciding or competing with hydride formation at moderately negative applied potentials, the desorption and solvation of possibly cleavable PtH$_n$ species, and the kinetic or thermodynamic stabilization of intermediates by cations through physisorption or intercalation will help understand the entire nature of cathodic corrosion on Pt(111).

SUPPLEMENTARY MATERIAL

See the supplementary material for statistical analysis of atomic charges in platinum hydride slabs, atomic structure output files of

platinum hydride slabs for VASP, and Pt–Pt interatomic distances between surface and subsurface Pt atoms in the platinum hydride slabs.

ACKNOWLEDGMENTS

AUTHOR DECLARATIONS

Conflict of Interest

The authors have no conflicts to disclose.

Author Contributions

Selwyn Hanselman: Conceptualization (equal); Data curation (equal); Formal analysis (equal); Investigation (equal); Methodology (equal); Writing – original draft (equal); Writing – review & editing (equal). **Federico Calle-Vallejo**: Supervision (equal); Writing – review & editing (equal). **Marc T. M. Koper**: Conceptualization (equal); Funding acquisition (equal); Supervision (equal); Writing – review & editing (equal).

DATA AVAILABILITY

The data that support the findings of this study are available within the article and its supplementary material and from the corresponding author upon reasonable request.

REFERENCES

[1] A. I. Yanson, P. Rodriguez, N. Garcia-Araez, R. V. Mom, F. D. Tichelaar, and M. T. M. Koper, Angew. Chem., Int. Ed. **50**, 6346 (2011).

[2] P. Rodriguez, F. D. Tichelaar, M. T. M. Koper, and A. I. Yanson, J. Am. Chem. Soc. **133**, 17626 (2011).

[3] T. J. P. Hersbach, C. Ye, A. C. Garcia, and M. T. M. Koper, ACS Catal. **10**, 15104 (2020).

[4] F. Haber, Z. Anorg. Chem. **16**, 438 (1898).

[5] T. J. P. Hersbach, A. I. Yanson, and M. T. M. Koper, Nat. Commun. **7**, 12653 (2016).

[6] S. Popović, M. Smiljanić, P. Jovanovič, J. Vavra, R. Buonsanti, and N. Hodnik, Angew. Chem., Int. Ed. **59**, 14736 (2020).

[7] B. Vanrenterghem, M. Bele, F. R. Zepeda, M. Šala, N. Hodnik, and T. Breugelmans, Appl. Catal., B **226**, 396 (2018).

[8] R. Otsuka and M. Uda, Corros. Sci. **9**, 703 (1969).

[9] E. Bennett, J. Monzó, J. Humphrey, D. Plana, M. Walker, C. McConville, D. Fermin, A. Yanson, and P. Rodriguez, ACS Catal. **6**, 1533 (2016).

[10] I. Evazzade, A. Zagalskaya, and V. Alexandrov, J. Phys. Chem. Lett. **13**, 3047 (2022).

[11] T. J. P. Hersbach, I. T. McCrum, D. Anastasiadou, R. Wever, F. Calle-Vallejo, and M. T. M. Koper, ACS Appl. Mater. Interfaces **10**, 39363 (2018).

[12] T. Scheler, O. Degtyareva, M. Marqués, C. L. Guillaume, J. E. Proctor, S. Evans, and E. Gregoryanz, Phys. Rev. B **83**, 214106 (2011).

[13] N. Hirao, F. Hiroshi, O. Yasuo, T. Kenichi, and K. Takumi, Acta Crystallogr., Sect. A: Found. Crystallogr. **64**, C609–C610 (2008).

[14] M. E. Martins, C. F. Zinola, G. Andreasen, R. C. Salvarezza, and A. J. Arvia, J. Electroanal. Chem. **445**, 135 (1998).

[15] K. A. Stoerzinger, M. Favaro, P. N. Ross, J. Yano, Z. Liu, Z. Hussain, and E. J. Crumlin, J. Phys. Chem. B **122**, 864 (2018).

[16] S. Hong, T. S. Rahman, R. Heid, and K. P. Bohnen, Surf. Sci. **587**, 41 (2005).

[17] P. Légaré, Surf. Sci. **559**, 169 (2004).

[18] C. Mager-Maury, G. Bonnard, C. Chizallet, P. Sautet, and P. Raybaud, ChemCatChem **3**, 200 (2011).

[19] G. Kresse and J. Furthmüller, Comput. Mater. Sci. **6**, 15 (1996).

[20] G. Kresse and J. Furthmüller, Phys. Rev. B **54**, 11169 (1996).

[21] G. Kresse and J. Hafner, Phys. Rev. B **47**, 558 (1993).

[22] G. Kresse and J. Hafner, Phys. Rev. B **49**, 14251 (1994).

[23] N. Arulmozhi, S. Hanselman, V. Tudor, X. Chen, D. van Velden, G. F. Schneider, F. Calle-Vallejo, and M. T. M. Koper, in *Observing What Cannot Be Observed: Computational Electrochemistry from Carbon to Hydrogen*, edited by S. Hanselman (Scholarly Publications Leiden University, Leiden, 2022), pp. 79–100.

[24] J. P. Perdew, K. Burke, and M. Ernzerhof, Phys. Rev. Lett. **77**, 3865 (1996).

[25] P. E. Blöchl, Phys. Rev. B **50**, 17953 (1994).

[26] G. Kresse and D. Joubert, Phys. Rev. B **59**, 1758 (1999).

[27] J. K. Nørskov, J. Rossmeisl, A. Logadottir, L. Lindqvist, J. R. Kitchin, T. Bligaard, and H. Jónsson, J. Phys. Chem. B **108**, 17886 (2004).

[28] J. Neugebauer and M. Scheffler, Phys. Rev. B **46**, 16067 (1992).

[29] H. J. Monkhorst and J. D. Pack, Phys. Rev. B **13**, 5188 (1976).

[30] W. Tang, E. Sanville, and G. Henkelman, J. Phys.: Condens. Matter **21**, 084204 (2009).

[31] A. van de Walle and G. Ceder, Phys. Rev. B **59**, 14992 (1999).

[32] S. Heiles and R. L. Johnston, Int. J. Quantum Chem. **113**, 2091 (2013).

[33] M. Jäger, R. Schäfer, and R. L. Johnston, Adv. Phys.: X **3**, 1516514 (2018).

[34] J. Zhang, V.-A. Glezakou, R. Rousseau, and M.-T. Nguyen, J. Chem. Theory Comput. **16**, 3947 (2020).

[35] R. Peverati and D. G. Truhlar, Philos. Trans. R. Soc., A **372**, 20120476 (2014).

[36] J. N. Mills, I. T. McCrum, and M. J. Janik, Phys. Chem. Chem. Phys. **16**, 13699 (2014).

[37] M. M. Elnagar, T. Jacob, and L. A. Kibler, Electrochem. Sci. Adv. (published online) (2021).

[38] M. M. Elnagar, J. M. Hermann, T. Jacob, and L. A. Kibler, Curr. Opin. Electrochem. **27**, 100696 (2021).

[39] M. D. Pohl, S. Watzele, F. Calle-Vallejo, and A. S. Bandarenka, ACS Omega **2**, 8141 (2017).

[40] N. Arulmozhi, T. J. P. Hersbach, and M. T. M. Koper, Proc. Natl. Acad. Sci. U. S. A. **117**, 32267 (2020).